nature immunology

Autotaxin, an ectoenzyme that produces lysophosphatidic acid, promotes the entry of lymphocytes into secondary lymphoid organs

Hidenobu Kanda[1], Rebecca Newton[1,3], Russell Klein[1,3], Yuka Morita[1,3], Michael D Gunn[2,3] & Steven D Rosen[1]

The extracellular lysophospholipase D autotaxin (ATX) and its product, lysophosphatidic acid, have diverse functions in development and cancer, but little is known about their functions in the immune system. Here we found that ATX had high expression in the high endothelial venules of lymphoid organs and was secreted. Chemokine-activated lymphocytes expressed receptors with enhanced affinity for ATX, which provides a mechanism for targeting the secreted ATX to lymphocytes undergoing recruitment. Lysophosphatidic acid induced chemokinesis in T cells. Intravenous injection of enzymatically inactive ATX attenuated the homing of T cells to lymphoid tissues, probably through competition with endogenous ATX and exertion of a dominant negative effect. Our results support the idea of a new and general step in the homing cascade in which the ectoenzyme ATX facilitates the entry of lymphocytes into lymphoid organs.

High endothelial venules (HEVs) in lymph nodes, Peyer's patches and other secondary lymphoid tissue contribute to continuous immune surveillance by supporting the recruitment of lymphocytes from the blood[1–3]. Considerable work has established that HEVs are morphologically and functionally specialized to capture lymphocytes circulating at high speed in the bloodstream and to support their migration into the lymphoid organ. HEVs are characterized by high endothelial cells (HECs) with a plump morphology and a well developed Golgi complex and rough endoplasmic reticulum[1]. Such features suggest highly active biosynthetic activities, whereas endothelial cells in other tissues generally have thin morphology and quiescent phenotypes. Sites of chronic inflammation can develop HEV-like vessels that also serve as a gateway for lymphocyte entry[2,4].

As is generally true for leukocyte-endothelium interactions, lymphocyte-HEV interactions occur in three sequential steps: rolling of lymphocytes along the endothelium, arrest on the endothelium and transmigration across the endothelium[1,3,5]. In lymph node HEVs, the rolling step is governed by weak and transient interactions between L-selectin on the lymphocyte and the carbohydrate determinant 'sialyl 6-sulfo Lewis X', which is presented by a family of sialomucin proteins on HEVs[2]. In homing to Peyer's patches, both L-selectin and the integrin $\alpha_4\beta_7$ interact with the $\alpha_4\beta_7$ ligand MAdCAM-1 on HEVs to support lymphocyte rolling[6]. The arrest step is induced by so-called 'arrest' chemokines such as CCL21 and CCL19 (also called SLC and ELC, respectively), which are immobilized and presented on the apical aspect of HEVs[3,7]. These molecules trigger activation of the integrin LFA-1 on lymphocytes and increase its affinity for its ligands ICAM-1 and ICAM-2, expressed on HEVs. The transendothelial migration step is poorly understood.

The knowledge gaps about HEV function have prompted several gene-profiling analyses of purified HECs from lymphoid organs[8–10]. An expressed sequence tag study of human tonsillar HEC gene expression has shown that about 5% of the transcripts encode the ectoenzyme autotoxin (ATX; A003157)[10]. ATX was originally identified in human melanoma cell culture medium as an autocrine motility factor that potently induces the motility of the melanoma cells[11,12]. ATX is overexpressed in various tumors and has been linked to tumor cell migration, invasiveness and metastasis[13]. ATX is required for normal development, as gene-targeted mice die *in utero* with profound defects in vascular formation and other abnormalities[14,15]. Notable in the sequence of ATX is a phosphodiesterase domain, which is required for its motility-stimulating activity[12,16]. Several years after its cloning, ATX was found to have lysophospholipase D activity, which generates lysophosphatidic acid (LPA) from lysophosphatidylcholine[17,18]. As an extracellular lysophospholipid, LPA elicits a wide variety of responses in many cell types through interactions with a family of five G protein–coupled receptors (GPCRs)[13,19]. Among its most extensively studied activities, LPA regulates cytoskeletal organization and migration in many cell types[13]. In several cases, it has been established that the motility-stimulating activity

[1]Department of Anatomy, Program in Immunology, Cardiovascular Research Institute, and [2]Cardiovascular Research Institute, University of California San Francisco, San Francisco, California 94143, USA. [3]Present addresses: Office of the Gene Technology Regulator, Federal Government Department of Health, Canberra 2601, Australia (R.N.), Pulmonary and Critical Care Medicine Division, University of California Irvine, Orange, California 92868, USA (R.K.), Osaka University Faculty of Medicine, Osaka 565-0871, Japan (Y.M.) and Department of Medicine, Division of Cardiovascular Medicine, Duke University, Durham, North Carolina 27710, USA (M.D.G.). Correspondence should be addressed to S.D.R. (steven.rosen@ucsf.edu).

Received 22 October 2007; accepted 8 February 2008; published online 9 March 2008; doi:10.1038/ni1573

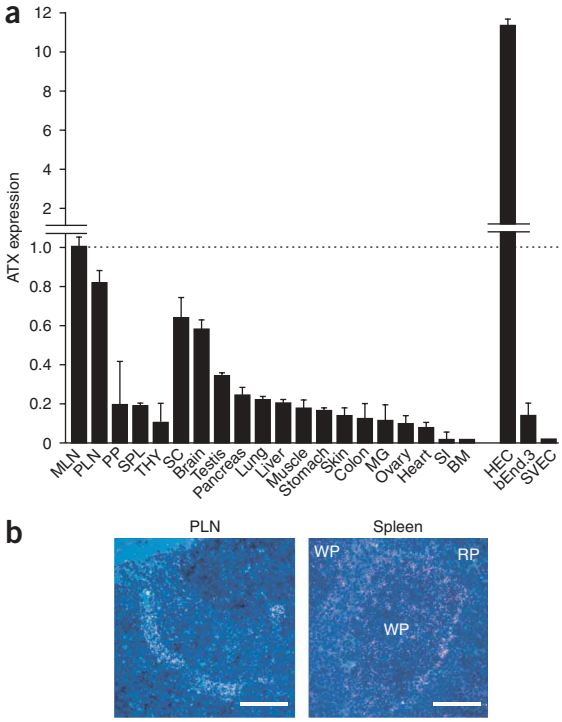

Figure 1 Expression of ATX transcripts by mouse tissues. (**a**) Quantitative PCR analysis of first-strand cDNA synthesized from RNA obtained from mouse tissues and cell populations. The abundance of ATX mRNA is normalized to that of hypoxanthine guanine phosphoribosyl transferase mRNA and is presented relative to the normalized amount in MLNs, set as 1. PP, Peyer's patch; SPL, spleen; THY, thymus; SC, spinal cord; MG, mammary gland; SI, small intestine; BM, bone marrow. Data (mean and s.d.) are based on analysis of three independent samples for each tissue type and cell type. (**b**) *In situ* hybridization analysis of ATX mRNA expression in PLNs and spleen with a ^{35}S-labeled mouse ATX antisense probe. Specific signals were not present in control samples analyzed with a sense probe (data not shown). RP, red pulp; WP, white pulp. Scale bars, 100 μm. Data are representative of two separate experiments with at least one lymphoid organ of each type examined at three exposure times.

of ATX is mediated through the production of LPA and signal transduction through its specific GPCRs[17,20].

Most interest in ATX has been directed toward its functions in cancer and early development. The discovery that HECs have high expression of ATX transcripts[10] prompted our investigation of the potential functions of this protein in the immune system. Our studies show a general contribution of ATX to the entry of lymphocytes from the blood into secondary lymphoid organs.

RESULTS

ATX expression in mouse lymph nodes

To explore the expression of ATX transcripts in lymphoid organs, we analyzed total RNA from a range of mouse tissues by real-time PCR. Consistent with published reports[13], we found that central nervous tissues such as brain and spinal cord had more abundant expression of ATX transcripts than did most other tissues (**Fig. 1a**). However, mesenteric lymph nodes (MLNs) and peripheral lymph nodes (PLNs) had the highest expression of all of the organs assessed. Notably, purified HECs from lymph nodes had 11-fold higher expression than did whole MLNs. The mouse endothelial cell line bEnd.3 also expressed the transcripts but much less so than did HECs. There was no detectable expression in SVEC, another mouse endothelial cell line.

We next did *in situ* hybridization to locate ATX transcripts in mouse lymph nodes. Consistent with expressed sequence tag results obtained with human HECs[10] and our real-time PCR measurements (**Fig. 1a**), an antisense probe to the gene encoding ATX strongly hybridized to HEVs of peripheral lymph nodes (**Fig. 1b**). The probe also selectively reacted with HEVs of Peyer's patches, a gut-associated lymphoid organ (data not shown). In the spleen, a lymphoid organ that lacks HEVs, hybridization signals were strongest in marginal zone regions, a chief site for the entry of lymphocytes into white pulp areas[21] (**Fig. 1b**).

We also did immunohistochemical analysis to determine the location of ATX protein in these tissues. We used an affinity-purified rabbit antibody to a 20–amino acid peptide of ATX (**Supplementary Fig. 1** online). To identify HEVs in lymph nodes, we used MECA-79, a monoclonal antibody that stains HEVs through its recognition of L-selectin ligands[2]. ATX was strongly expressed in MECA-79$^+$ HEVs in both MLNs and PLNs (**Fig. 2**). Peyer's patch HEVs were also ATX$^+$ (data not shown). Some smaller vessel-like structures, which were MECA-79$^-$ and lacked a high wall morphology, were ATX$^+$ (**Fig. 2**, arrowheads). We confirmed these structures as vessels by their positive staining for the endothelial marker CD31 (data not shown). In the spleen, we confirmed that central arterioles (CD31$^+$) and marginal zones were strongly ATX$^+$. To investigate ATX expression at sites of lymphoid neogenesis (so-called 'tertiary lymphoid organs'), we used the nonobese diabetic and rat insulin promoter–B lymphocyte chemokine mouse models, in which pancreata have HEV-like vessels in association with lymphoid aggregates[4]. We detected ATX expression in MECA-79$^+$ HEV-like vessels in both models (**Supplementary Fig. 2** online). In all cases, staining was not present when the antibody to ATX was incubated with the peptide immunogen or when an isotype control antibody was used (**Supplementary Fig. 1**).

Secretion of ATX by HECs

ATX was originally thought to be a type II membrane protein that could be released extracellularly by proteolysis of a plasma membrane-associated precursor[13]. However, ATX has now been shown to be a true secretory protein with a cleavable signal sequence[22,23]. To determine whether HECs secrete ATX, we isolated this population of cells from disaggregated mouse lymph nodes using immunomagnetic beads coupled to MECA-79. We separated proteins in conditioned medium from cultured HECs by SDS-PAGE and analyzed them by immunoblot with the antibody to ATX (**Fig. 3a**). The HEC culture supernatant and the crude stromal preparation had a reactive protein of 110 kilodaltons, which is the appropriate mass predicted for ATX. This signal was not present in medium conditioned by the HEC-depleted stroma or by lymphocytes. We used GlyCAM-1, a secretory product of HECs[2], as a positive control. To establish that the reactive component was indeed ATX, we isolated cDNA encoding ATX from an HEC cDNA library and transfected it into COS-7 African green monkey kidney cells. Immunoblot analysis of the purified recombinant ATX identified a prominent band whose migration was almost identical to that of the reactive species from HEC culture supernatant. These observations show that HECs synthesize and secrete ATX and establish that these cells are a principal ATX-producing population in lymph nodes.

We next addressed whether the secretion of ATX from HECs occurred more prominently from the apical or basolateral surface of the cells. As purified HECs do not organize into a continuous monolayer and rapidly lose their specialized gene expression pattern in

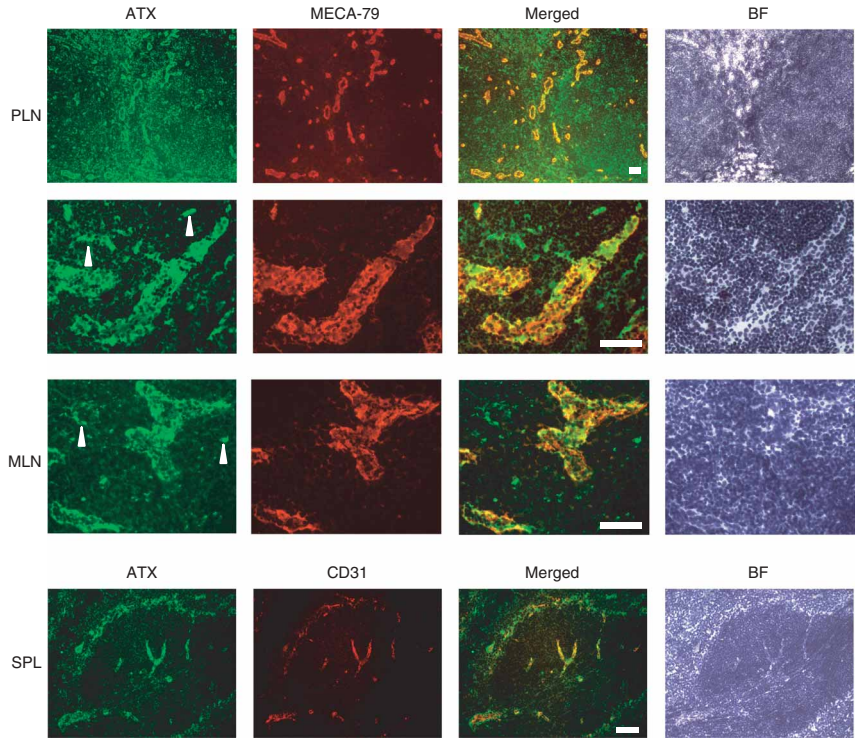

Figure 2 Localization of ATX protein in lymphoid organs. Two-color immunofluorescence of cryostat sections of PLNs and MLNs for ATX (green) and MECA-79 (red) and on spleen sections for ATX (green) and CD31 (red). Far right, brightfield (BF) images (hematoxylin staining) of the fields at left. White arrowheads indicate ATX$^+$ small vessels, which are MECA-79$^-$. Scale bars, 100 μm. Data are representative of four independent experiments.

culture[24], we used transfected MDCK canine kidney cells for these studies. MDCK cells form a highly polarized and tight monolayer and are widely used to study polarized secretion in epithelial cells[25]. We prepared a stable MDCK transfectant that expressed ATX with a six-histidine tag at the amino terminus. These cells established a tight monolayer, as confirmed by measurement of the passage of fluorescein isothiocyanate–dextran across the cell layer (**Fig. 3b**). We collected culture medium from above the monolayer (apical) and below the monolayer (basolateral) and assessed ATX by both immunoblot analysis and measurement of enzymatic activity (lysophospholipase D). By both measures, ATX was secreted mainly (over 90%) into the apical compartment (**Fig. 3c,d**). We also assessed the endogenous protein clusterin (Clstr; also called ApoJ), which is secreted in the apical direction by MDCK cells[25]. We found that 70–80% of clusterin was in the top compartment for both parental cells and the ATX-transfected line. On the basis of these results, we conclude that HECs secrete ATX apically and thus would add this protein to the blood. In fact, ATX is known to be present in blood plasma and serum, and these fluids have served as sources for its purification[17,18]. It remains to be determined whether HEVs in various lymphoid organs, as well as ATX$^+$ vessels in the spleen, are the main sources of ATX in the blood.

Binding of ATX to lymphocytes

As our results indicated apical secretion of ATX from HEVs, we next sought to determine whether there is a mechanism for targeting the activity of this ectoenzyme onto lymphocytes undergoing recruitment into lymphoid organs. ATX has many potential integrin-binding motifs, including an Arg-Gly-Asp sequence for interaction with $\alpha_5\beta_1$, $\alpha_V\beta_3$ and $\alpha_V\beta_5$ and a Leu-Asp-Val sequence for binding $\alpha_4\beta_1$ (ref. 26). We first explored whether soluble ATX could bind to peripheral blood lymphocytes in suspension. With a flow cytometry–based assay, we were able to detect binding to these cells in the presence of Mn^{2+} (a general enhancer of integrin activity[26]) in some experiments, but the signal was highly variable (data not shown). We next determined if ATX could serve as binding substrate for lymphocytes in a standard adhesion assay for integrin-dependent interactions, in which we coated ATX onto plastic wells. Jurkat T cells showed considerable adhesion to immobilized ATX in the presence of Mn^{2+} and much less interaction when Mn^{2+} was omitted (**Fig. 4a**). Consistent with previous findings[26], Mn^{2+} also enhanced the binding of Jurkat cells to ICAM-1 and VCAM-1, the endothelial ligand for the integrin $\alpha_4\beta_1$. Antibodies to the α_4 and β_1 subunits of $\alpha_4\beta_1$ substantially blocked the adhesion of Jurkat cells to ATX, whereas a function-blocking antibody to the β_2 integrin subunit and an irrelevant class-matched antibody had no effect (**Fig. 4b**). To determine whether a more physiological activator of integrins would increase the binding of Jurkat cells to ATX, we exposed lymphocytes to immobilized CCL21, an 'arrest' chemokine[3,7]. CCL21 stimulated greater adhesion of Jurkat cells to ATX, and this interaction required $\alpha_4\beta_1$ (**Fig. 4c**). In addition, overnight treatment of Jurkat cells with the phorbol ester PMA resulted in $\alpha_4\beta_1$-dependent adhesion of Jurkat cells to ATX (data not shown). Purified human T cells (isolated from peripheral blood) also bound to immobilized ATX. Mn^{2+} enhanced this interaction, as did coimmobilized CCL21, by about twofold. ATX was similar to VCAM-1 in its support of T cell adhesion per unit of input protein (**Fig. 4d**). Again, antibody blockade indicated involvement of $\alpha_4\beta_1$ in the interactions enhanced by CCL21 and Mn^{2+}, although inhibition by antibody to α_4 or β_1 was not as strong as it was for Jurkat cells (**Fig. 4e,f**), possibly because T cells have lower $\alpha_4\beta_1$ expression[27]. Unexpectedly, even though mouse lymphocytes had considerable binding to immobilized ATX (which could be inhibited by EDTA), we were unable to block this interaction with integrin-directed antibodies (specific for β_1, β_2 or α_4) or with integrin-binding peptides (Leu-Asp-Val and Arg-Gly-Asp; **Supplementary Fig. 3** online). Combinations of these antibodies were also ineffective.

Effects of LPA on lymphocytes

A chief enzymatic product of ATX is LPA. Because ATX was able to bind to lymphocytes (**Fig. 4**) and its substrate lysophosphatidylcholine is abundant in blood plasma[13], we next explored the effect of LPA on lymphocytes. LPA has been reported to stimulate cytoskeletal reorganization of actin in T cell lymphoma cell lines[28]. We used a fluorescent conjugate of phalloidin to measure the effects of LPA on actin polymerization in purified human T cells. LPA (5 μM) induced an increase of 40% in intracellular filamentous actin within 15 min of its addition (**Fig. 5a**). This increase was comparable to that induced in

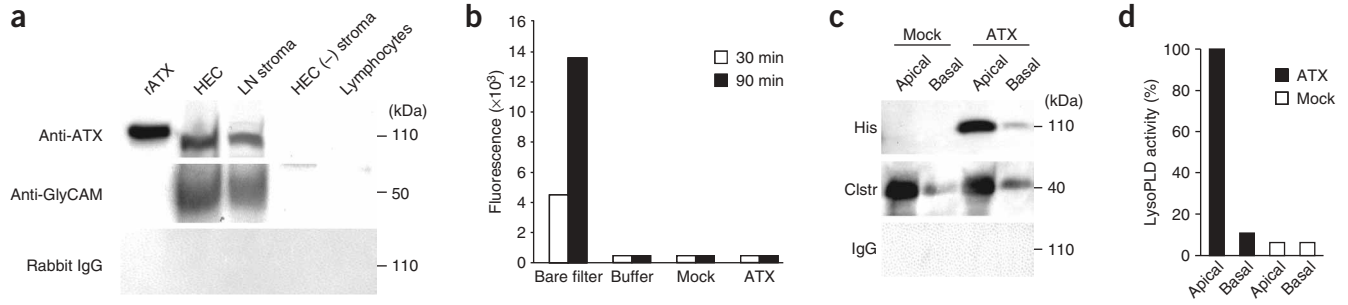

Figure 3 Secretion of ATX by HECs and transfected MDCK cells. (**a**) Immunoblot analysis of ATX and GlyCAM-1 in conditioned medium from isolated HECs. The slight difference in the molecular weights of recombinant ATX (rATX) and native ATX is probably due to glycosylation differences. LN, lymph node; HEC (–), no HECs; kDa, kilodaltons. Bottom, membrane stripped and reprobed with normal rabbit IgG as a control. (**b**) Transwell assay of the diffusion of fluorescein isothiocyanate–dextran across MDCK monolayers (ATX transfected or 'mock' transfected) for analysis of monolayer integrity. Far left, diffusion across a bare filter. (**c**,**d**) Immunoblot analysis (**c**) and ATX enzymatic activity analysis (lysophospholipase D (LysoPLD)) (**d**) of supernatants collected from above (Apical) or below (Basal) MDCK monolayers. (**c**) Analysis of ATX (histidine tag (His)) or clusterin (Clstr); below, control mouse IgG. Data are representative of three (**a**) or two (**b**–**d**) independent experiments.

eosinophils by the same concentration of LPA[29]. In agreement with published work[30], CXCL12, a highly active chemokine for lymphocytes, also elicited actin polymerization in the T cells (**Fig. 5a**).

LPA promotes the invasiveness of T cell lymphomas into fibroblast monolayers[28]. Additionally, in a Transwell assay, LPA has been found to induce both the chemotaxis and the chemokinesis of Jurkat T cells engineered to express mainly the LPA_2 GPCR for LPA[31]. To determine whether LPA had motility-enhancing effects on primary human T cells, we did a conventional Transwell assay. When LPA was added to the top well with lymphocytes, it stimulated migration to the lower well with the greatest effect at a concentration of 1 μM (**Fig. 5b**). This chemokinetic activity was inhibited by pretreatment of the lymphocytes with pertussis toxin, consistent with the involvement of a G protein of the G_i family (**Fig. 5c**). To test for chemotactic activity, we added LPA to the lower well alone. This had no effect on the migration of the lymphocytes (**Fig. 5d**). Also, the addition of LPA at the same concentration to both wells produced the same effect as the addition of LPA to the upper well, consistent with a chemokinetic action of LPA. The inability of LPA in the lower chamber to induce responses from lymphocytes may have reflected its nonspecific binding to the

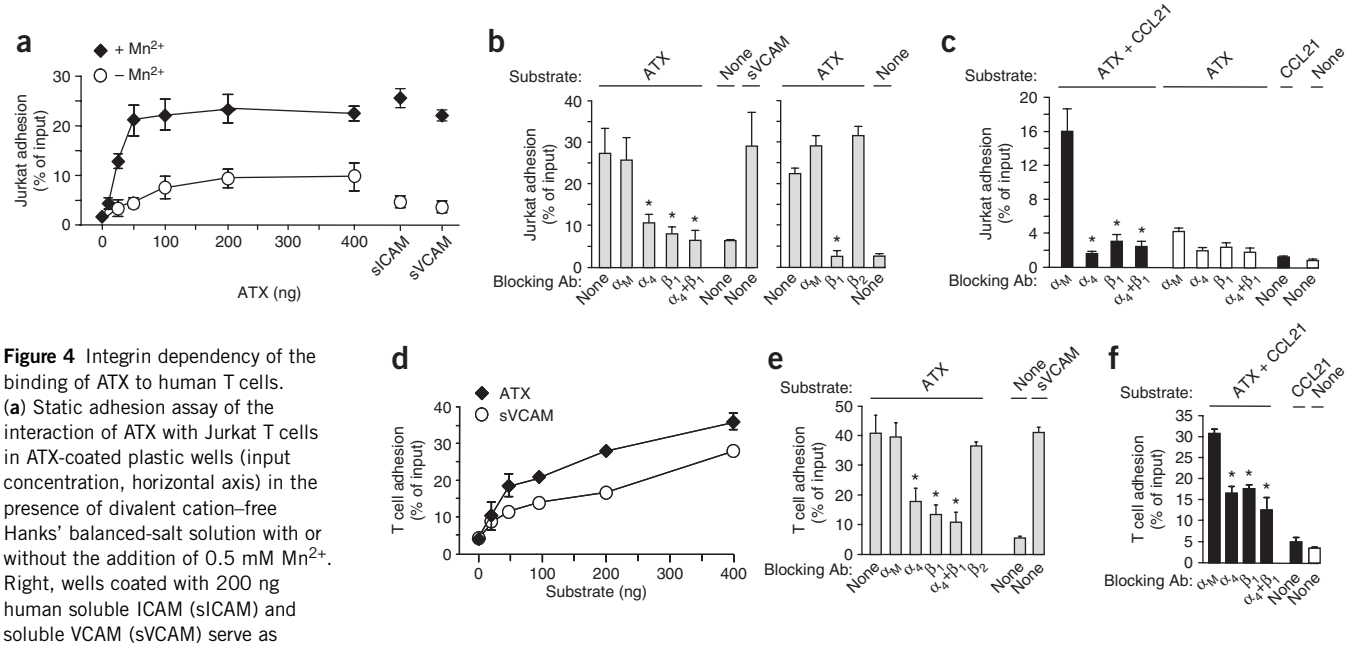

Figure 4 Integrin dependency of the binding of ATX to human T cells. (**a**) Static adhesion assay of the interaction of ATX with Jurkat T cells in ATX-coated plastic wells (input concentration, horizontal axis) in the presence of divalent cation–free Hanks' balanced-salt solution with or without the addition of 0.5 mM Mn^{2+}. Right, wells coated with 200 ng human soluble ICAM (sICAM) and soluble VCAM (sVCAM) serve as positive controls for adhesive substrates. (**b**) Adhesion analysis of Jurkat T cells pretreated with function-blocking antibody for integrin α_M, α_4, β_1 or β_2 (Blocking Ab; 5 μg/ml) in buffer containing Mn^{2+}, tested for adhesion to ATX (200 ng). sVCAM, adhesion to wells coated with 200 ng VCAM-1. (**c**) Static adhesion assay of Jurkat T cells allowed to interact with various combinations (above graph) of ATX (200 ng) and CCL21 (100 ng) coated onto the plate. Filled bars, CCL21; open bars, no CCL21. (**d**) Binding of human T cells to wells coated with ATX or VCAM-1 (substrate concentration, horizontal axis) in the presence of Mn^{2+}. (**e**) Effect of function-blocking antibodies to integrin subunits on the adhesion of human T cells to wells coated with ATX (200 ng) in the presence of Mn^{2+}. sVCAM, adhesion to wells coated with 200 ng VCAM-1. (**f**) Interaction of ATX with primary human T cells exposed to CCL21 and ATX immobilized together as described in **c**, assessed after treatment of cells with function-blocking antibodies. *, $P < 0.01$, inhibitory effect of antibody relative to control. Data (mean ± s.d. of triplicate determinations) are representative of three to four experiments (**a**–**c**), two experiments (**b**, left and right; **d**,**f**) or one experiment (**e**).

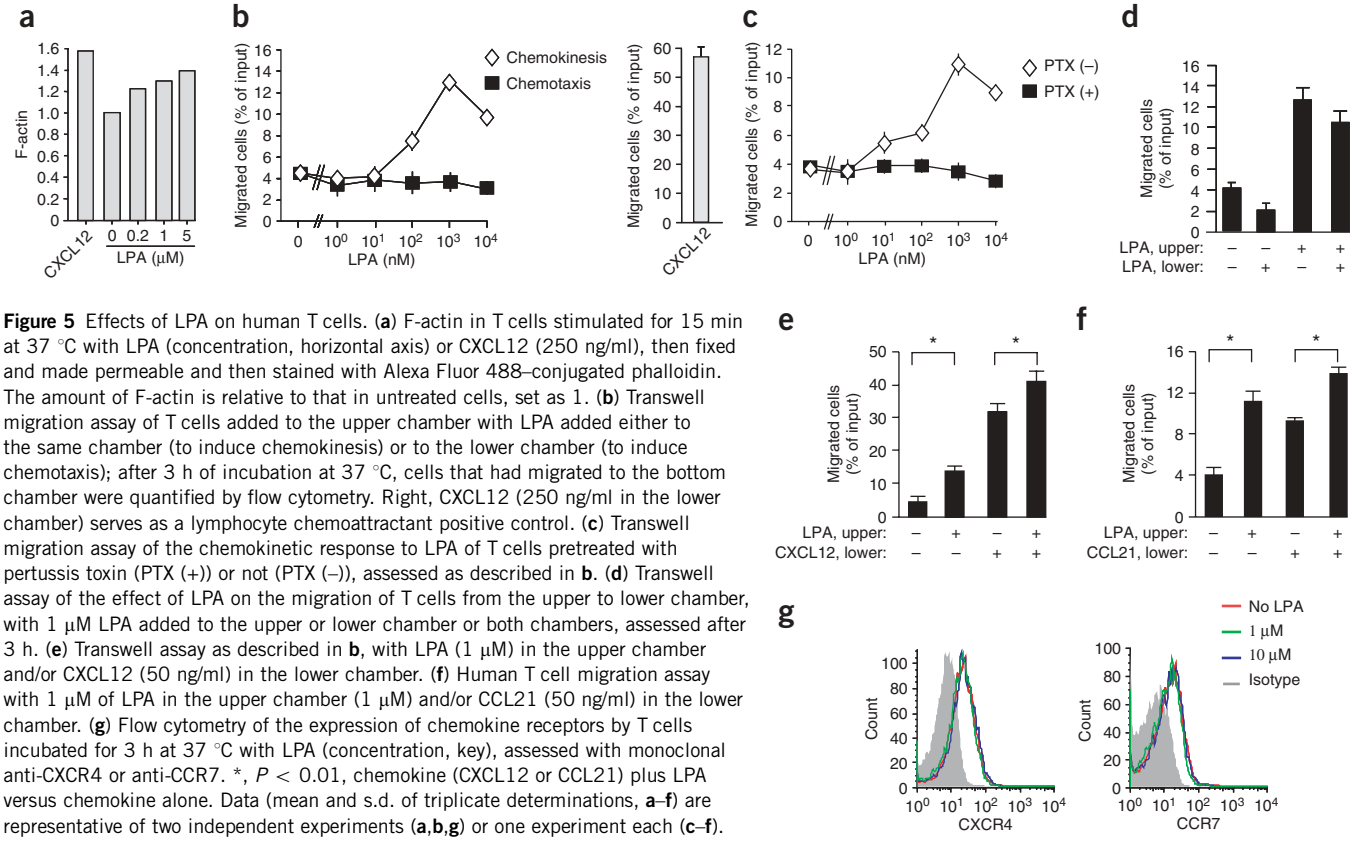

Figure 5 Effects of LPA on human T cells. (**a**) F-actin in T cells stimulated for 15 min at 37 °C with LPA (concentration, horizontal axis) or CXCL12 (250 ng/ml), then fixed and made permeable and then stained with Alexa Fluor 488–conjugated phalloidin. The amount of F-actin is relative to that in untreated cells, set as 1. (**b**) Transwell migration assay of T cells added to the upper chamber with LPA added either to the same chamber (to induce chemokinesis) or to the lower chamber (to induce chemotaxis); after 3 h of incubation at 37 °C, cells that had migrated to the bottom chamber were quantified by flow cytometry. Right, CXCL12 (250 ng/ml in the lower chamber) serves as a lymphocyte chemoattractant positive control. (**c**) Transwell migration assay of the chemokinetic response to LPA of T cells pretreated with pertussis toxin (PTX (+)) or not (PTX (–)), assessed as described in **b**. (**d**) Transwell assay of the effect of LPA on the migration of T cells from the upper to lower chamber, with 1 μM LPA added to the upper or lower chamber or both chambers, assessed after 3 h. (**e**) Transwell assay as described in **b**, with LPA (1 μM) in the upper chamber and/or CXCL12 (50 ng/ml) in the lower chamber. (**f**) Human T cell migration assay with 1 μM of LPA in the upper chamber (1 μM) and/or CCL21 (50 ng/ml) in the lower chamber. (**g**) Flow cytometry of the expression of chemokine receptors by T cells incubated for 3 h at 37 °C with LPA (concentration, key), assessed with monoclonal anti-CXCR4 or anti-CCR7. *, $P < 0.01$, chemokine (CXCL12 or CCL21) plus LPA versus chemokine alone. Data (mean and s.d. of triplicate determinations, **a**–**f**) are representative of two independent experiments (**a**,**b**,**g**) or one experiment each (**c**–**f**).

plastic filter[31]. When we added a known chemotactic factor (CXCL12 or CCL21) to the lower well, its effects were additive with those of LPA. Thus, with LPA in the upper well and CXCL12 or CCL21 in the lower well, migration to the lower well was greater than with LPA alone in the upper well or chemoattractant alone in the lower well (**Fig. 5e**,**f**). We obtained similar results with mouse lymphocytes (**Supplementary Fig. 4** online). To determine whether LPA might have been increasing the expression of receptors for CXCL12 or CCL21, we measured surface expression of CXCR4 and CCR7 on T cells after LPA treatment. There was no change in the amount of these receptors (**Fig. 5g**). We conclude that lymphocytes are able to respond simultaneously to the chemokinetic action of LPA and the chemotactic action of chemokines.

Effect of inactive ATX on T cell homing

The presence of receptor sites for ATX on activated lymphocytes, together with the ability of LPA to stimulate lymphocyte migration, suggested a potential function for ATX during lymphocyte homing. In this paracrine model (**Supplementary Fig. 5** online), ATX is secreted into the lumens of HEVs and binds to adherent lymphocytes through an interaction with an activated receptor ($\alpha_4\beta_1$ is one example). ATX may first bind to HEVs and subsequently interact with lymphocytes as an immobilized ligand. Next, the lymphocyte-bound ATX acts on its abundant substrate lysophosphatidylcholine in the blood and catalyzes the production of a high local concentration of LPA, which triggers GPCRs on the lymphocyte and promotes transendothelial migration. This model allows the prediction that an excess of catalytically inactive ATX in the blood could potentially act in a dominant negative way by competing with endogenous ATX for a limited number of ATX-binding sites on the lymphocyte. To test that proposal, we prepared a mutant of ATX with a single amino acid change in the phosphodiesterase domain (T210A)[16] and analyzed it together with the wild-type protein (**Supplementary Fig. 6** online). As expected, lysophospholipase D activity was absent for the mutant and was readily detected for the wild-type protein. We found that the T210A mutant was equivalent to wild-type ATX in its ability to support the adhesion of Mn^{2+}-stimulated lymphocytes (**Supplementary Fig. 6**). We tested the effects of these two proteins in a standard lymphocyte-homing assay. We labeled purified T lymphocytes with fluorescence, mixed with them with inactive or active ATX or with PBS and then injected them intravenously into wild-type mice. After 15 min, we determined by flow cytometry the number of fluorescent cells that had accumulated in lymph nodes, Peyer's patches and spleen (**Fig. 6a**). Relative to PBS treatment, inactive ATX (4 μg per mouse) attenuated the homing of T cells to lymph nodes and Peyer's patches by 50–60% and their homing to the spleen by 30%. Active ATX at the same concentration did not affect homing to any organ. The lower accumulation of lymphocytes was not due to removal of lymphocytes from the blood, as treatment with inactive ATX had no effect on the number of labeled lymphocytes in the blood. Increasing the amount of inactive ATX to 8 μg per mouse did not augment inhibition (data not shown).

To visualize the effects of ATX on the migration of lymphocytes into and within lymphoid organs, we collected lymph nodes 15 min after injection of labeled lymphocytes and evaluated the numbers and positions of fluorescent cells in sections. Consistent with the homing measurements, treatment of lymphocytes with mutant ATX (4 μg per mouse) decreased the total number of lymphocytes in the lymph sections by 50% or more relative to treatment with the active ATX or PBS (**Fig. 6b**). To compare the effects of the two proteins on overall lymphocyte migration, we assessed the positions of individual cells

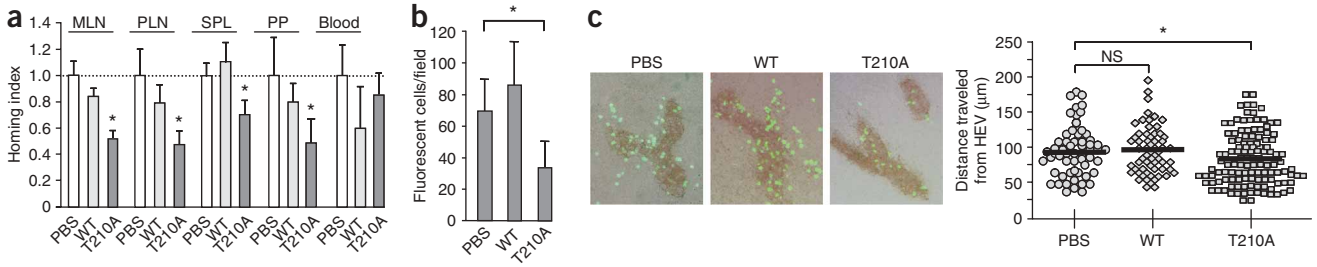

Figure 6 Migration of T cells to and within lymphoid organs in the presence of exogenous ATX. (**a**) Flow cytometry of CFSE-labeled T cells pretreated with PBS, active ATX (WT) or enzymatically inactive ATX (T210A) and injected intravenously (4 μg active or inactive ATX per mouse) into recipient mice, then quantified 15 min later in tissues from recipient mice. For lymphoid organs, $n = 6$ mice (PBS) and $n = 8$ mice (active and inactive ATX); for blood, $n = 4$ mice (each condition). Values are relative to those of PBS, set as 1. *, $P < 0.01$, versus PBS control. Data are representative of five experiments (mean and s.d. of results pooled from two experiments). (**b**) Entry of lymphocytes into PLNs, assessed in cryostat sections of lymph nodes processed 15 min after injection of labeled lymphocytes into mice treated as described in **a**; total lymphocytes were counted in at least ten nonsequential sections for each treatment ($n = 3$ mice per treatment condition). Data (mean and s.d.) are representative of two independent experiments. (**c**) Lymphocyte migration within PLNs, assessed by measurement of the distance between extravasated lymphocytes (outside HEVs) and the nearest HEV in lymph nodes processed 15 min after injection of fluorescent lymphocytes into mice treated as described in **a**; HEVs are identified by staining with MECA-79. Left, microscopy of cryosatat sections; right, distances measured in ten nonsequential sections ($n = 3$ mice for each treatment condition). Original magnification, ×20. *, $P < 0.05$; NS, nonsignificant. Data are representative of two independent experiments.

relative to the nearest HEV (visualized by MECA-79 staining) and determined the distance migrated. Mutant ATX inhibited overall migration relative to treatment with PBS or wild-type ATX (**Fig. 6c**). Thus, the introduction of a low concentration of inactive ATX into the circulation caused a general decrease in the homing of lymphocytes to secondary lymphoid organs and impeded the dispersal of lymphocytes in at least one type of organ.

DISCUSSION

Despite the fact that naive lymphocytes are intrinsically nonmotile in standard *in vitro* conditions[32], these cells constitutively enter lymphoid organs. Culture of lymphocytes together with HECs promotes the efficient passage of lymphocytes across the endothelial layer, which suggests HECs express a 'lymphocyte migration stimulus'[33,34]. Although a soluble factor that corresponds to this activity has been described[34], the biochemical identity and mechanism of action of this 'stimulus' have not been defined. We report here that ATX is a likely candidate for the postulated lymphocyte motility stimulus.

Following up on earlier gene profiling analysis of HECs[10], we found here that that mouse lymphoid organs had abundant expression of ATX transcripts and confirmed that HECs were a particularly rich source of this. We confirmed the expression of ATX protein in lymph node HEVs by immunocytochemistry and biochemical analysis of isolated HECs. We also found ATX expression in HEV-like vessels in two different models of lymphoid neogenesis. Many proteins expressed by HEVs (including selectin ligand scaffolding proteins, fucosyltransferases, sulfotransferases and chemokines), which are critically involved in the lymphocyte homing cascade, are elements of an HEV differentiation program[4]. Lymphotoxin signaling is required for this program during organogenesis and for the induction of HEV-like vessels at sites of lymphoid neogenesis[4,35]. Notably, the gene encoding ATX is one of a limited subset of genes suppressed in lymph nodes by blockade of lymphotoxin signaling[36], which suggests that it may be an element of the HEV differentiation program.

Our finding that ATX was secreted by HECs in an apical orientation indicated a possible parallel with 'arrest' chemokines. These are secreted by HEVs, become associated with apical receptors and exert their effects on adherent lymphocytes[7]. Noting a potential $\alpha_4\beta_1$-binding motif (Leu-Asp-Val) in the sequence of ATX, we sought to determine whether ATX could bind to lymphocytes through $\alpha_4\beta_1$. Indeed, we found that Jurkat cells and primary human T cells activated in three different ways showed $\alpha_4\beta_1$-dependent adhesion to immobilized ATX. This finding suggests that ATX could be targeted to HEV-adherent lymphocytes whose integrins have been activated during the arrest step of the recruitment cascade. Many $\alpha_4\beta_1$ ligands are known, including fibronectin, VCAM-1 and osteopontin[37]. ATX also has an Arg-Gly-Asp sequence, which suggests that ATX may be able to 'partner' with other integrins[26]. Further experiments are needed to define the nature of the divalent cation–dependent ATX receptors on mouse lymphocytes. It is conceivable that the versatility of ATX may include the ability to bind simultaneously to both HEV and lymphocyte, which could help 'bridge' the lymphocyte to the endothelium.

To arrive at a rationale for how ATX might influence lymphocyte activity, we examined the effects of LPA on primary T cells. We focused on LPA because many of the biological activities of ATX can be attributed to its production of this phospholipid[13]. Moreover, ATX accounts for the basal concentration of LPA in the blood[14,15]. Published reports have investigated the responses of lymphocytes (usually lymphoma populations) to LPA[19,28,31,38–40]. Most pertinent to our work here was the rapid action of LPA in inducing chemokinesis of Jurkat cells[31] and in promoting shape change and invasiveness of mouse lymphoma lines[28]. Our experiments with primary lymphocytes were consistent with those cell line studies[28,31]. Thus, we have shown that LPA induced actin polymerization in suspended cells and was chemokinetic in a Transwell assay. The dose-response curves were similar to those reported for LPA in other bioassays[17,20,31]. Notably, the optimal concentration for LPA in our experiments (about 1 μM) exceeds the basal concentration in blood plasma for both mice and humans[13–15]. We found that the chemokinetic effect of LPA was additive with the chemoattractant effects of CXCL12 and CCL21, which suggests the possibility of 'cooperative' interactions between LPA and chemokine signaling in migrating lymphocytes.

We obtained our most convincing functional results in short-term homing experiments. We found that intravenous injection of an enzymatically inactive form of ATX blocked the homing of blood-borne lymphocytes to lymph nodes, spleen and Peyer's patches. Our model posits that the inactive ATX would interfere with the function

of endogenous ATX by displacing it from a limited number of binding sites on lymphocytes (and possibly HECs), thus exerting a dominant negative effect. The endogenous ATX is proposed to emanate from HEVs. For spleen, the proposed sources are marginal zones, which surround white pulp regions and are known sites of lymphocyte entry. The net result of this competition from the inactive ATX would be less locally produced LPA and consequently less lymphocyte entry. Whether LPA affects cell motility, cell adhesion (for example, effects on LFA-1 after arrest), cell shape or transendothelial migration during the complex process of entry remains to be investigated. It should be noted that locally produced LPA at the lymphocyte-HEV nexus could also have effects on HEV function during lymphocyte recruitment, as LPA is able to elicit responses in endothelial cells[41].

The activity of ATX in regulating lymphocyte migration may extend beyond the entry phase, as we detected ATX in stromal regions of lymphoid organs. Lymphocytes show considerable motility in lymphoid organs, much of it apparently random in direction[3,21,42,43]. The chemokine receptor CCR7 and its chemokine ligand CCL21 account for a portion of T cell motility, probably through a chemokinetic effect[44–47]. LPA is a plausible candidate as an additional motility-stimulating factor in lymphoid organs. We found that treatment of mice with inactive ATX caused a decrease in the distance between labeled lymphocytes and the nearest HEVs. Whether this effect can be attributed to delayed entry into the lymph node or less motility in the node is not known. As for a possible contribution by ATX to the egress of lymphocytes from lymph nodes, we did not detect ATX in vessels positive for the lymphatic endothelial cell marker LYVE-1 (data not shown). Finally, it should be noted that ATX may be stably tethered to lymphoid stromal elements and thus could provide an adhesive substrate for migrating lymphocytes.

LPA signals cells through five known GPCRs (LPA_1–LPA_5), the first three of which (LPA_1, LPA_2 and LPA_3) are members of the 'EDG' family to which the sphingosine 1-phosphate receptors also belong[19,48,49]. Lymphocytes express mainly LPA_1 (refs. 40,48), LPA_2 (refs. 38,48) and LPA_5 (ref. 48), with subset 'preferences'. Unlike chemokine GPCRs, which signal mainly through G proteins of the G_i family[21], LPA receptors can use a variety of G protein families, including the G_i family[19]. We found that the LPA-induced chemokinesis of lymphocytes was blocked by pertussis toxin, which indicated involvement of G_i proteins in this response. However, pertussis toxin has no effect on lymphoma invasiveness, whereas G proteins of the G_q and G_{12}-G_{13} families have been linked to this response[28]. The LPA signaling pathways involved in lymphocyte migration into and within lymphoid organs remain to be identified.

The recruitment of lymphocytes into lymphoid organs is a multistep process. The molecular elucidation of this process over the past 20 years represents a triumph of immunology. Here we have proposed a new step in this process involving the regulation of lymphocyte migration by the ectoenzyme ATX. Our model of ATX action lends itself to testing with genetically engineered mice and pharmacological agents. As inhibitors of the exit of lymphocytes from lymphoid organs are of clinical value for achieving immunosuppression[19], inhibitors of the proposed ATX pathway may also be of therapeutic value in some settings by preventing entry of lymphocytes into secondary lymphoid organs or into induced tertiary lymphoid organs at sites of chronic inflammation[50].

METHODS

Human subjects. Peripheral venous blood was obtained from normal donors after they provided informed consent with approval from Committee for Human Research at the University of California, San Francisco. For some experiments, human T cells were prepared from peripheral blood purchased from Blood Centers of the Pacific (San Francisco).

Mice. All mouse experiments were in accordance with protocols approved by the Committee for Animal Research of the University of California, San Francisco. For real-time PCR, C57BL/6 female mice (8 weeks of age) were used for RNA extraction. For homing assays, CD-1 female mice (6–8 weeks of age) were used as both recipient and donor mice. Mice were from Charles River Laboratories.

Reagents, antibodies and proteins. Fatty acid–free BSA, L-α-lysophosphatidic acid, L-α-lysophosphatidylcholine, choline oxidase and peroxidase were from Sigma. The polyclonal antibody used for immunocytochemistry was prepared by immunization of rabbits with the peptide CKKPDQHFKPYMKQHLPKRL (ProSci) and purification of the resultant serum on a peptide affinity column as described[51]. The specificity of the antibody was confirmed by enzyme-linked immunosorbent assay and peptide inhibition (**Supplementary Fig. 1**). A published antibody to ATX directed against the same peptide sequence[51] was used for immunoblot analysis of ATX. Other antibodies are described below. Recombinant human and mouse VCAM-immunoglobulin fusion proteins were from R&D Systems. Recombinant human CXCL12 and human CCL21 were from Leinco Technologies.

Cells. HECs purified from mouse lymph nodes were prepared as described[9,10]. Mouse T cells were prepared from CD-1 mouse MLNs and PLNs. Samples were depleted of non–T cells with mouse and human Pan T Cell Isolation kits (Miltenyi Biotec). At least 98% of the resulting cells expressed CD3. Jurkat T cells were maintained in RPMI-1640 medium (Mediatech) supplemented with 10% (vol/vol) FBS (Invitrogen), penicillin (100 units/ml), streptomycin (100 μg/ml) and 2-mercaptoethanol (25 μM).

Cloning of human cDNA encoding ATX and expression of ATX protein. Full-length cDNA encoding ATX was cloned from a human tonsil HEC library[52] by a pool-selection technique in conjunction with PCR, based on published procedures[52]. The cDNA was sequenced in both directions and the protein encoded exactly matched the teratocarcinoma form of human ATX, which differs from melanoma ATX in lacking a 52–amino acid insertion. Native ATX produced by melanoma cells has an amino terminus beginning at residue 49 (ref. 12). A cDNA construct encoding a 51-residue amino-terminal-truncated version of ATX was cloned into the pSecTag expression vector (Invitrogen) with a six-histidine tag at the amino terminus. PCR-based mutagenesis was used for the preparation of cDNA encoding enzymatically inactive ATX in which the critical amino acid residue threonine at position 210 was replaced with alanine (T210A)[16]. Proteins were purified from supernatants of transfected COS-7 cells by chromatography on nickel–nitrilotriacetic acid sepharose (Qiagen). The purified proteins produced a single band by both gel staining (GelCode, Pierce) and immunoblot analysis after SDS-PAGE. Protein concentrations were determined by the Bradford assay with BSA as the standard.

ATX secretion assay. For analysis of ATX secreted from purified HECs, conditioned medium was prepared by culture of HECs for 96 h in Opti-MEM I (Invitrogen) with concentration by Vivaspin (Vivascience). Proteins from conditioned medium were separated by SDS-PAGE (2 μg/lane; 4–20% gradient gel; Bio-Rad) in reducing conditions and were transferred to ProBlott membranes (Applied Biosystems). After blockade with 3% (wt/vol) BSA in PBS, filters were probed with antibody to ATX or with antibody to GlyCAM-1 (ref. 53), followed by biotin-conjugated goat antibody to rabbit immunoglobulin (goat anti–rabbit IgG; 111-065-008; Jackson ImmunoResearch) and streptavidin–horseradish peroxidase (Jackson ImmunoResearch) with chemiluminescent detection (GE Healthcare). MDCK cells stably transfected with ATX were prepared by transfection with the ATX pSecTag vector mentioned above using FuGENE 6 (Roche) followed by selection in Zeocin (0.5 mg/ml; Invitrogen). MDCK cells were cultured for 4 d in Transwell chambers (pore size, 0.4 μm; Corning) to allow confluent monolayers to form. The medium was replaced with Opti-MEM I and cells were cultured for an additional 4 d. Supernatants from the upper and lower chambers were analyzed for lysophospholipase D activity and were separated by SDS-PAGE and analyzed by immunoblot. Antibodies to a five-histidine tag (MCA1396; AbD Serotec) and

clusterin (SC-6419; Santa Cruz) were used as primary antibodies, followed by horseradish peroxidase–conjugated secondary antibodies with detection by enhanced chemiluminescence. The membrane used for analysis with the monoclonal antibody to the five-histidine tag was stripped and reprobed with mouse IgG (02-6502; Zymed) as a control.

Real-time PCR. Total RNA was extracted from tissues of three 8-week-old female C57BL/6 mice by Trizol (Invitrogen) and was subjected to reverse-transcription with Superscript II reverse transcriptase (Invitrogen) and random hexamers (Invitrogen). Real-time PCR was done in the Biomolecular Resource Center at University of California, San Francisco with a 7900HT TaqMan (Applied Biosystems). For measurement of ATX mRNA expression, the following primer set and probe were used: forward primer, 5′-TGTGGAAGGC AGCTCTATTCCTGT-3′; reverse primer, 5′-ATTGTCAGGTCGGTGAG GAAG GAT-3′; probe, 5′-(5-carboxyfluorescein)-ACTTCACTCAGCCTGCAGACA AGTGT-(black-hole quencher)-3′. PCR conditions were as follows: 10 min at 95 °C, then 40 cycles of 15 s at 95 °C and 2 min at 60 °C. Results were analyzed with SDS 2.1 software. ATX expression was normalized to that of hypoxanthine guanine phosphoribosyl transferase.

***In situ* hybridization.** Paraffin sections (5 μm in thickness) of peripheral lymph nodes from C57BL/6 mice were deparaffinized, were fixed in 4% (vol/vol) paraformaldehyde and were treated with proteinase K. After being washed in saline citrate buffer, sections were incubated in hybridization solution overnight with sense or antisense ^{35}S-labeled ATX riboprobe[52]. After hybridization, sections were washed, were dipped in photographic emulsion NTB2 (Kodak), were developed and were counterstained with hematoxylin and eosin.

Immunofluorescence. Mouse tissues were embedded and frozen in optimum cutting temperature compound. Cryostat sections 10 μm in thickness were fixed in acetone and blocked with 3% (wt/vol) BSA in PBS containing 10% (vol/vol) goat serum, then were stained with anti-ATX as a primary antibody, followed by biotin-conjugated goat anti–rabbit IgG and carbocyanine-streptavidin (016-220-084; Jackson ImmunoResearch Laboratories). For simultaneous MECA-79 staining, indocarbocyanine-labeled goat anti–rat IgM (112-165-075; Jackson ImmunoResearch Laboratories) was used as a secondary detection antibody. Digital images were captured with an Optiphot microscope (Nikon) equipped with a digital camera system (AxioCam; Zeiss).

Lysophospholipase D assay. Lysophospholipase D activity was measured as described[17]. ATX protein was incubated for up to 4 h at 37 °C with 1 mM lysophosphatidylcholine and the choline liberated was assessed colorimetrically by linked reactions with choline oxidase (2 U/ml) and peroxidase (5 U/ml).

Static ATX adhesion assay. Wells of a 96-well Immulon 2HB (Thermo) plate were coated overnight at 4 °C with ATX in Mg^{2+}- and Ca^{2+}-free PBS. After the plates were rinsed with PBS, free binding sites were blocked for 2 h at 22 °C with 0.2% (wt/vol) polyvinylpyrrolidone (molecular weight, 360 kilodaltons; Sigma). When Mn^{2+} was used for the assay, Jurkat T cells or human peripheral blood T cells labeled with 5-chloromethylfluorescein diacetate (Invitrogen) were pretreated for 30 min at 22 °C with antibody at a concentration of 5 μg/ml in Hanks' balanced-salt solution containing 25 mM HEPES, pH 7.4, 0.5 mM Mn and 0.5% BSA (fatty acid–free). For CCL21 stimulation, ATX (200 ng) and CCL21 (100 ng) were immobilized together on wells as described above. Cells were then added to wells and were allowed to settle for 1 h at 37 °C. After nonadherent cells were removed by inversion of the plate, adherent cells were made soluble with 0.2% (vol/vol) Nonidet P-40 in PBS and the fluorescence of the wells was measured with a Cytofluor II (Perseptive Biosystems). The following function-blocking antibodies were used: ICRF44 (α_M subunit; 301311; BioLegend), HP2/1 (α_4 subunit; MAB1383; Chemicon), P5D2 (β_1 subunit; SC-13590; Santa Cruz) and TS1/18 (β_2 subunit; 302111; BioLegend).

Transwell assay. Human T cells (1×10^6) were added to the upper chambers of Transwells (pore size, 5 μm; Costar) and were allowed to migrate for 3 h at 37 °C. For analysis of the chemokinetic response of T cells, cells were incubated with various concentrations of LPA in the upper chamber. In some experiments, CXCL12 or CCL21 was simultaneously added to the lower chambers. For pertussis toxin inhibition experiments, T cells were preincubated for 2–3 h at 37 °C with pertussis toxin (250 ng/ml; Fluka). Migrated cells were quantified by flow cytometry.

F-actin-reorganization assay. Purified T cells were incubated for 15 min at 37 °C with or without LPA. Cells were fixed and made permeable in PBS containing 2% (vol/vol) paraformaldehyde and 0.2% (vol/vol) Triton X-100 and were stained with Alexa Fluor 488–conjugated phalloidin (Invitrogen). The incorporation of fluorescent phalloidin into T cells was analyzed by flow cytometry.

Chemokine receptor expression. The expression of chemokine receptors by T cells was assessed by flow cytometry. T cells were treated for 3 h at 37 °C with LPA, then were incubated with anti-CXCR4 (12G5; 555972; BD Pharmingen), anti-CCR7 (3D12; 552175; BD Pharmingen) or isotype-matched control IgG (02-6502; Zymed). Cells were incubated with phycoerythrin-conjugated secondary antibody (Jackson ImmunoResearch Laboratories) and were analyzed by flow cytometry.

***In vivo* T cell–homing assay.** Purified T cells from PLNs and MLNs of 6- to 8-week-old CD-1 mice were labeled for 30 min at 37 °C with the cytosolic dye CFSE (carboxyfluorescein diacetate succinimidyl ester; Invitrogen). Cells were incubated for 2 h at 37 °C with ATX protein (wild-type or inactive; 40 μg/ml) or with PBS. Human ATX protein was used; it is 94% identical to mouse ATX. Cells (5×10^7) in 100 μl of PBS plus ATX protein (total, 4 μg) were injected through the tail vein into age-matched CD-1 recipient mice. Then, 15 min later, mice were killed and suspensions of MLNs, PLNs, Peyer's patches and spleen were prepared by mechanical dissociation. Blood samples were also collected. $CFSE^+$ cells in each sample were quantified by flow cytometry (as $CFSE^+$ cells per 1×10^6 total lymphocytes for MLNs, PLNs, spleen and blood or $CFSE^+$ cells per 5×10^5 total cells for Peyer's patches). Data were acquired with CellQuest (BD Bioscience) and analyzed with FlowJo (Tree Star). For analysis of the number and distribution of injected lymphocytes in lymph nodes, frozen blocks were prepared after mice were killed and sections 10 μm in thickness were prepared and fixed with 4% (vol/vol) parafornaldehyde. Fluorescent cells in many fields were counted in ten nonsequential sections. For identification of HEVs, sections were stained with biotin-conjugated MECA-79 followed by streptavidin–horseradish peroxidase and NovaRED (Vector). For analysis of the distance between fluorescent cells and HEVs, fluorescent cells outside HEVs were identified and the distance to the center of the nearest HEV was measured for many lymphocytes in each section for at least ten different nonsequential sections. Measurements were made by investigator 'blinded' to sample identity.

Statistical analysis. The Student's *t*-test was used for statistical analysis.

Accession code. UCSD-Nature Signaling Gateway (http://www.signaling-gateway.org): A003157.

Note: Supplementary information is available on the Nature Immunology website.

ACKNOWLEDGMENTS

We thank B. Fuss (Virginia Commonwealth University Medical Center) for polyclonal anti–rat ATX; J.G. Cyster (University of California, San Francisco) for monoclonal anti–mouse α_4 and anti–mouse α_L and for rat insulin promoter–B lymphocyte chemokine mice; J. Bluestone (University of California, San Francisco) for nonobese diabetic mice; M. Singer and D. Tsay for assistance with homing assays; and E.J. Goetzl and J.G. Cyster for advice and critical reading of this manuscript. Supported by the National Institute of Health (RO1-GM57411 and RO1-GM23547 to S.D.R.) and the Uehara Memorial Foundation, Japan (H.K.).

AUTHOR CONTRIBUTIONS

H.K. and S.D.R. conceptualized and designed the research and prepared the manuscript; S.D.R. supervised the research and provided intellectual guidance; H.K. did experiments and analyzed data; R.N. and R.K. participated in the early phases of this project; Y.M. quantified ATX homing; and M.D.G. supervised the *in situ* hybridization.

Published online at http://www.nature.com/natureimmunology
Reprints and permissions information is available online at http://npg.nature.com/reprintsandpermissions

1. Miyasaka, M. & Tanaka, T. Lymphocyte trafficking across high endothelial venules: dogmas and enigmas. *Nat. Rev. Immunol.* **4**, 360–370 (2004).
2. Rosen, S.D. Ligands for L-selectin: homing, inflammation, and beyond. *Annu. Rev. Immunol.* **22**, 129–156 (2004).
3. von Andrian, U.H. & Mempel, T.R. Homing and cellular traffic in lymph nodes. *Nat. Rev. Immunol.* **3**, 867–878 (2003).
4. Drayton, D.L., Liao, S., Mounzer, R.H. & Ruddle, N.H. Lymphoid organ development: from ontogeny to neogenesis. *Nat. Immunol.* **7**, 344–353 (2006).
5. Ley, K., Laudanna, C., Cybulsky, M. & Nourshargh, S. Getting to the site of inflammation: the leukocyte adhesion cascade updated. *Nat. Rev. Immunol.* **7**, 678–689 (2007).
6. Butcher, E.C. & Picker, L.J. Lymphocyte homing and homeostasis. *Science* **272**, 60–66 (1996).
7. Ley, K. Arrest chemokines. *Microcirculation* **10**, 289–295 (2003).
8. Girard, J.-P. & Springer, T.A. Cloning from purified high endothelial venule cells of hevinl a close relative of the antiadhesive extracellular matrix protein SPARC. *Immunity* **2**, 113–123 (1995).
9. Izawa, D. *et al.* Expression profile of active genes in mouse lymph node high endothelial cells. *Int. Immunol.* **11**, 1989–1998 (1999).
10. Palmeri, D., Zuo, F.R., Rosen, S.D. & Hemmerich, S. Differential gene expression profile of human tonsil high endothelial cells: implications for lymphocyte trafficking. *J Leuk. Biol.* **75**, 910–927 (2004).
11. Stracke, M.L. *et al.* Identification, purification, and partial sequence analysis of autotaxin, a novel motility-stimulating protein. *J. Biol. Chem.* **267**, 2524–2529 (1992).
12. Murata, J. *et al.* cDNA cloning of the human tumor motility-stimulating protein, autotaxin, reveals a homology with phosphodiesterases. *J. Biol. Chem.* **269**, 30479–30484 (1994).
13. Mills, G.B. & Moolenaar, W.H. The emerging role of lysophosphatidic acid in cancer. *Nat. Rev. Cancer* **3**, 582–591 (2003).
14. Tanaka, M. *et al.* Autotaxin stabilizes blood vessels and is required for embryonic vasculature by producing lysophosphatidic acid. *J. Biol. Chem.* **281**, 25822–25830 (2006).
15. van Meeteren, L.A. *et al.* Autotaxin, a secreted lysophospholipase D, is essential for blood vessel formation during development. *Mol. Cell. Biol.* **26**, 5015–5022 (2006).
16. Lee, H.Y. *et al.* Stimulation of tumor cell motility linked to phosphodiesterase catalytic site of autotaxin. *J. Biol. Chem.* **271**, 24408–24412 (1996).
17. Umezu-Goto, M. *et al.* Autotaxin has lysophospholipase D activity leading to tumor cell growth and motility by lysophosphatidic acid production. *J. Cell Biol.* **158**, 227–233 (2002).
18. Tokumura, A. *et al.* Identification of human plasma lysophospholipase D, a lysophosphatidic acid-producing enzyme, as autotaxin, a multifunctional phosphodiesterase. *J. Biol. Chem.* **277**, 39436–39442 (2002).
19. Goetzl, E.J. & Rosen, H. Regulation of immunity by lysosphingolipids and their G protein-coupled receptors. *J. Clin. Invest.* **114**, 1531–1537 (2004).
20. Hama, K. *et al.* Lysophosphatidic acid and autotaxin stimulate cell motility of neoplastic and non-neoplastic cells through LPA1. *J. Biol. Chem.* **279**, 17634–17639 (2004).
21. Cyster, J.G. Chemokines, sphingosine-1-phosphate, and cell migration in secondary lymphoid organs. *Annu. Rev. Immunol.* **23**, 127–159 (2005).
22. Jansen, S. *et al.* Proteolytic maturation and activation of autotaxin (NPP2), a secreted metastasis-enhancing lysophospholipase D. *J. Cell Sci.* **118**, 3081–3089 (2005).
23. Koike, S., Keino-Masu, K., Ohto, T. & Masu, M. The N-terminal hydrophobic sequence of autotaxin (ENPP2) functions as a signal peptide. *Genes Cells* **11**, 133–142 (2006).
24. Baekkevold, E.S. *et al.* Culture characterization of differentiated high endothelial venule cells from human tonsils. *Lab. Invest.* **79**, 327–336 (1999).
25. Cohen, D., Rodriguez-Boulan, E. & Musch, A. Par-1 promotes a hepatic mode of apical protein trafficking in MDCK cells. *Proc. Natl. Acad. Sci. USA* **101**, 13792–13797 (2004).
26. Ruoslahti, E. RGD and other recognition sequences for integrins. *Annu. Rev. Cell Dev. Biol.* **12**, 697–715 (1996).
27. Kitani, A. *et al.* Soluble VCAM-1 induces chemotaxis of Jurkat and synovial fluid T cells bearing high affinity very late antigen-4. *J. Immunol.* **161**, 4931–4938 (1998).
28. Stam, J.C., Michiels, F., van der Kammen, R.A., Moolenaar, W.H. & Collard, J.G. Invasion of T-lymphoma cells: cooperation between Rho family GTPases and lysophospholipid receptor signaling. *EMBO J.* **17**, 4066–4074 (1998).
29. Idzko, M. *et al.* Lysophosphatidic acid induces chemotaxis, oxygen radical production, CD11b up-regulation, $Ca^{2.}$ mobilization, and actin reorganization in human eosinophils via pertussis toxin-sensitive G proteins. *J. Immunol.* **172**, 4480–4485 (2004).
30. Bleul, C.C., Fuhlbrigge, R.C., Casasnovas, J.M., Aiuti, A. & Springer, T.A. A highly efficacious lymphocyte chemoattractant, stromal cell-derived factor 1 (SDF-1). *J. Exp. Med.* **184**, 1101–1109 (1996).
31. Zheng, Y., Kong, Y. & Goetzl, E.J. Lysophosphatidic acid receptor-selective effects on Jurkat T cell migration through a Matrigel model basement membrane. *J. Immunol.* **166**, 2317–2322 (2001).
32. Wilkinson, P.C. The locomotor capacity of human lymphocytes and its enhancement by cell growth. *Immunology* **57**, 281–289 (1986).
33. Ager, A. Regulation of lymphocyte migration into lymph nodes by high endothelial venules. *Biochem. Soc. Trans.* **25**, 421–428 (1997).
34. Harris, H. The stimulation of lymphocyte motility by cultured high endothelial cells and its inhibition by pertussis toxin. *Int. Immunol.* **3**, 535–542 (1991).
35. Browning, J.L. *et al.* Lymphotoxin-β receptor signaling is required for the homeostatic control of HEV differentiation and function. *Immunity* **23**, 539–550 (2005).
36. Huber, C. *et al.* Lymphotoxin-β receptor-dependent genes in lymph node and follicular dendritic cell transcriptomes. *J. Immunol.* **174**, 5526–5536 (2005).
37. Bayless, K.J. & Davis, G.E. Identification of dual $\alpha_4\beta_1$ integrin binding sites within a 38 amino acid domain in the N-terminal thrombin fragment of human osteopontin. *J. Biol. Chem.* **276**, 13483–13489 (2001).
38. Goetzl, E.J., Kong, Y. & Voice, J.K. Cutting edge: differential constitutive expression of functional receptors for lysophosphatidic acid by human blood lymphocytes. *J. Immunol.* **164**, 4996–4999 (2000).
39. Rieken, S. *et al.* Lysophospholipids control integrin-dependent adhesion in splenic B cells through G_i and G_{12}/G_{13} family G-proteins, but not through G_q/G_{11}. *J. Biol. Chem.* **281**, 36985–36992 (2006).
40. Zheng, Y., Voice, J.K., Kong, Y. & Goetzl, E.J. Altered expression and functional profile of lysophosphatidic acid receptors in mitogen-activated human blood T lymphocytes. *FASEB J.* **14**, 2387–2389 (2000).
41. Wu, H.-L. *et al.* Lysophosphatidic acid stimulates thrombomodulin lectin-like domain shedding in human endothelial cells. *Biochem. Biophys. Res. Commun.* **367**, 162–168 (2008).
42. Miller, M.J., Wei, S.H., Parker, I. & Cahalan, M.D. Two-photon imaging of lymphocyte motility and antigen response in intact lymph node. *Science* **296**, 1869–1873 (2002).
43. Bajenoff, M. *et al.* Highways, byways and breadcrumbs: directing lymphocyte traffic in the lymph node. *Trends Immunol.* **28**, 346–352 (2007).
44. Worbs, T., Mempel, T.R., Bolter, J., von Andrian, U.H. & Forster, R. CCR7 ligands stimulate the intranodal motility of T lymphocytes in vivo. *J. Exp. Med.* **204**, 489–495 (2007).
45. Okada, T. & Cyster, J.G. CC chemokine receptor 7 contributes to Gi-dependent T cell motility in the lymph node. *J. Immunol.* **178**, 2973–2978 (2007).
46. Huang, J.H. *et al.* Requirements for T lymphocyte migration in explanted lymph nodes. *J. Immunol.* **178**, 7747–7755 (2007).
47. Woolf, E. *et al.* Lymph node chemokines promote sustained T lymphocyte motility without triggering stable integrin adhesiveness in the absence of shear forces. *Nat. Immunol.* **8**, 1076–1085 (2007).
48. Kotarsky, K. *et al.* Lysophosphatidic acid binds to and activates GPR92, a G protein-coupled receptor highly expressed in gastrointestinal lymphocytes. *J. Pharmacol. Exp. Ther.* **318**, 619–628 (2006).
49. Lee, C.W., Rivera, R., Gardell, S., Dubin, A.E. & Chun, J. GPR92 as a new $G_{12/13}$- and G_q-coupled lysophosphatidic acid receptor that increases cAMP, LPA_5. *J. Biol. Chem.* **281**, 23589–23597 (2006).
50. Luster, A.D., Alon, R. & von Andrian, U.H. Immune cell migration in inflammation: present and future therapeutic targets. *Nat. Immunol.* **6**, 1182–1190 (2005).
51. Fox, M.A., Collello, R.J., Macklin, W.B. & Fuss, B. Phosphodiesterase-Ialpha/autotaxin: a counteradhesive protein expressed by oligodendrocytes during onset of myelination. *Mol. Cell. Neurosci.* **23**, 507–519 (2003).
52. Bistrup, A. *et al.* Sulfotransferases of two specificities function in the reconstitution of high-endothelial-cell ligands for L-selectin. *J. Cell Biol.* **145**, 899–910 (1999).
53. Lasky, L.A. *et al.* An endothelial ligand for L-selectin is a novel mucin-like molecule. *Cell* **69**, 927–938 (1992).